μ-Si strain gauge array on flexible substrate for dynamic pressure measurement

F. Garcia Castro, O. de Sagazan, N Coulon, A. Homs Corbera, D. Fassini, J. Cramer, F. Le Bihan

µ-Si Strain Gauge Array on Flexible Substrate for Dynamic Pressure Measurement.

Fatima Garcia Castro*, Olivier de Sagazan*, Nathalie Coulon*, Antoni Homs Corbera**, Dario Fassini**, Jeremy Cramer**, France Le Bihan*.

* Univ Rennes, CNRS, IETR, UMR 6164, F-35000 Rennes, France

**Cherry Biotech, 35000 Rennes

Corresponding author: O de Sagazan
Olivier.de-sagazan@univ-rennes1.fr 0033 2 23 23 52 67

Abstract

Low Temperature µ-Si layers have been deposited by Inductively Coupled Plasma Chemical Vapour Deposition (ICP-CVD) to produce strain gauges. These strain gauges performed on 25µm thick flexible Kapton Polyimide (PI) were investigated in terms of Gauge Factor but also in dynamic mode through a homemade pneumatic test bench. Best strain gauge design has been identified and subsequently used to perform a 25 sensor array which was also tested using pulses and more complex signals. A simulation of blood pressure monitoring was performed to demonstrate the value of the technology.

Author Keywords

ICP-CVD; PECVD; Strain Gauges Array; TLM; µ-Si Doped; Flexible Electronics; Thin Film Pressure Sensor, Dynamic Pressure Measurement, Blood Pressure monitoring.

1. Introduction

Flexible electronics is today a major research field due to a growing market. Many devices on flexible substrates are under development with promising prospects in robotics [1], health monitoring [2], epidermal electronics [3], intelligent textile [4] or photovoltaic. Most resistive strain sensors are limited in sensitivity and especially when high spatial resolution is required. Therefore, the aim of this work is to develop sensor array on flexible substrate able to measure small local deformations with a spatial accuracy and dynamically in a 0.1-10Hz range.

Two main types of materials are used as strain gauges: metals and semiconductors. Other materials such as organic semi-conductors [5], graphite [6], carbon nanotubes [7] or conductive polymer composites [8] are discussed in the literature but are not yet mature. The gauge factor (*GF*) is typically used to quantify the sensitivity of a resistive strain sensor and is defined by **Eq. (1)** as the ratio of the relative change of its electrical resistance ($\Delta R/R_0$) and the strain ε applied to that sensor:

$$GF = \frac{\Delta R/R_0}{\varepsilon} \qquad (1)$$

For metals, *GF* is low, between 2 to 5 [9], and their low resistivity implies long wires for measurable values and is a limitation to reach accurate spatial resolution. For semiconductors, especially silicon-based materials, *GF* exhibits much higher values due to the so-called piezoresistivity effect: 100 for single crystalline silicon (sc-Si), 20–40 for polycrystalline silicon (poly-Si) [10] or 20–30 for amorphous silicon (a-Si) [11]. The possibility of controlling their resistivity by doping is also an advantage when designing measurable resistors in limited spaces.

Silicon films can be deposited in an amorphous or crystallized state by plasma enhanced chemical vapour deposition (PECVD) at low temperature (< 250 °C). Microcrystalline silicon (µ-Si) with a grain size around 20nm and a crystal fraction higher than 50% is more stable and can lead to higher electrical performances. High quality µ-Si or nano-crystalline-Si:H deposited at low temperature could be achieved by PECVD by diluting H_2, Ar and SiH_4 [12]. Indeed, in the past, some researches have been carried out to investigate the effect of Ar dilution on the deposition of amorphous and microcrystalline silicon by PECVD. Some interesting results have been obtained in this way, leading to TFT realization by PECVD below 200°C using µ-Si from PECVD [13].

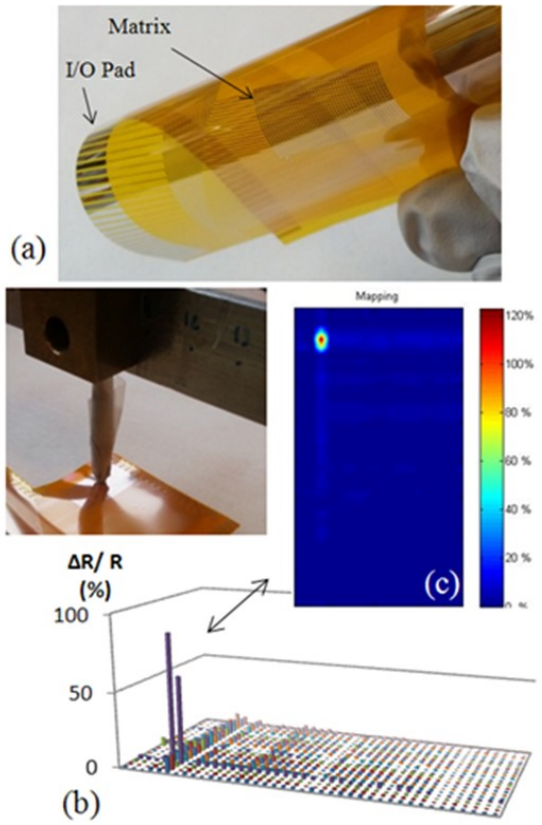

Figure1. a) 800 sensor array performed in µ-Si PECVD on 50µm thick Kapton (PI) with the pressure test device applying a 1,9N/mm² stress, b) ΔR/R variation and pressure mapping realised with a sub-millimetre ball applied on matrix, c) Matlab visualisation of the resistance variation [14].

Strain gauges using a directly deposited µ-Si film as piezoresistive material on a 50 µm thick polyimide (PI) substrate, have been performed by PECVD in H_2/Ar dilution and investigated [14]. In this previous work, strain gauges issue from PECVD were studied individually with tensile and compressive bending tests at large applied bending (down to 5 mm bendinfg

radii) by Transmission Line Method to directly extrapolate the resistivity of the µc-Si film and associated GF [14]. In the same work, strain gauges were implemented in an 800 sensor array (Figure 1), demonstrating the potential of this technology to perform high accuracy mapping pressure. All these results were obtained with static measurements, the monitoring of 800 sensors in dynamic mode being too complex to implement.

Based on the background get on these µ-Si strain gauges using PECVD, it was decided, in the framework of the present work, to explore the dynamic behaviour of µ-Si sensors on flexible substrates performed by ICP-CVD. In this paper, µ-Si doped strain gauges were deposited on 25µm PI (Kapton) sheets. After determination of the ICP-CVD µ-Si GF, two designs of strain gauges were dynamically investigated to define the best geometry that could be used to realize a 25 sensor array. Sensitivity and reliability of the sensor array were determined to show main advantages of this matrix approach. Finally, a test simulating blood pressure monitoring was performed to show the interest of µ-Si sensors technology on flexible substrate.

2. ICP-CVD µ-Si characterization and static Gauge Factor measurement

The use of Inductively Coupled Plasma Chemical Vapour Deposition (ICP-CVD) to perform Si layers at low temperature appears to be very interesting and several works report on this method. Some TFTs have been fabricated using ICP-CVD for either active semiconductor or insulator deposition. This method has been widely used for a-Si targeting solar cell application [15-16-17] and especially to create a-Si/µ-Si heterojunctions [18] for solar cell yield improvement. ICP-CVD process is also used in SiC deposition [19], and finds some application in Micro Electro Mechanical Systems MEMS fields [20]. Doped layers issue from ICP-CVD have been reported [21], with boron and for solar cell applications, it generally leads to rather high resistivity value even with N type dopant such as phosphorous [22]. These works report dilution of AsH_3 and PH_3 in H_2 and SiH_4. Use of H_2 dilution has already been investigated [23] but it does not seem that SiH_4+Ar+H_2 mixture have been used for the realization of µ-Si strain gauges in ICP-CVD as we proposed in the following study.

2.1 ICP-CVD µ-Si layers conditions:

The ICP-CVD Corial 210D machine is a reactor using pure SiH_4 combined with carrier gases such as H_2, Ar. It is possible to add PH_3, AsH_3 and B_2H_6 to perform in-situ doping. For the insulator process, it is also possible to add N_2 or NH_3 to the plasma for nitride, O_2 or N_2O directly for oxide deposition. A CF_4 line gas is also available to clean the reactor chamber by CF_4/O_2 plasma. The machine has two generators, one dedicated to RF plasma, and the other for ICP power, which could reach 1000 W. Both generators as also mass flows could be monitored in pulsed mode. The pumping system is able to achieve the process at 2 mTorr (depending on carrier gas flow level) and substrates from 2 to 6 inches can be processed. In this work, active layer of strain gauges have been realized with a µ-Si deposited at 185°C with a SiH_4/H_2/Ar mixture. Layers are N-type doped by adding PH_3 during deposition only ICP generator is in operation (LF 600W Low Frequency) and no RF power is applied. The resistivity obtained reaches 0.1 Ohm.cm under conditions on PI films.

2.2 Gauge Factor Measurement:

The GF determination is based on the Transmission Line Method (TLM) [24]. In order to quantify the piezoresistive effect, strain gauges are measured while the substrate is bent with different radii of curvature *r*. In our bending test bench [14], TLM structures are measured and, it results for different radii, different resistances according applied strain. Figure 2 shows the homemade tools and the set up used to study tensile stresses. According samples, 4 or 5 bending radii (2.5, 2, 1.5, 1, 0.5 cm) were used. The study focused on the longitudinal *GF*, so the length *L* of the resistors was perpendicular to the bending axis i.e. the current flow was parallel to the bending direction.

For each radius of curvature, the strain applied to the structure is calculated using a bi-layer model as a function of their Young's modulus value *Y* [25], (Figure 3).

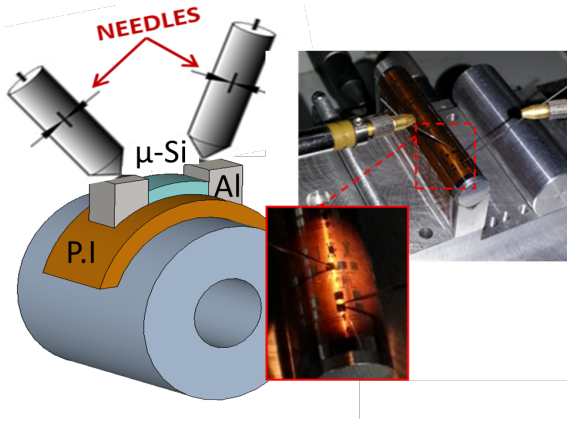

Figure 2. Homemade tools (steel cylinders) used for static I-V TLM measurements under bending for tensile tests.

In our case, material properties are presented in Table 1. The Al electrodes are not schown since we focus on the µ-Si channel of the resistor, between the 2 contacts. The bi-layer model is thus constituted by the PI substrate and the µ-Si layer.

Layer	PI	µc-Si
Thickness	25 µm	100 nm
Y (GPa)	2.5 [26]	80 [27]

Table 1. Material properties used in this paper.

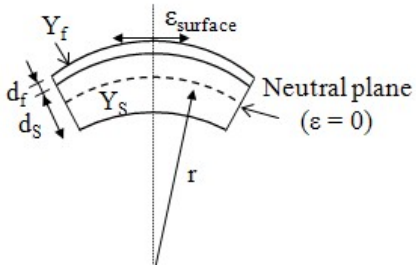

Figure 3. Schematic cross-section of the mechanical model. The names refer to **Eq. (2)**.

The longitudinal strain $\varepsilon_{surface}$ on the surface of the top layer is given by the equation derived from [27]:

$$\varepsilon_{surface} = \left(\frac{d_f + d_s}{2r} \right) \frac{\left(1 + 2\chi\eta + \chi\eta^2\right)}{(1+\eta)(1+\chi\eta)} \text{ Where}$$

$$\eta = \frac{d_f}{d_s} \text{ and } \chi = \frac{Y_f}{Y_s} \quad (2)$$

where r is the applied radii of curvature, d_S and d_f are substrate and layer thicknesses respectively, χ and η are defined by $\chi = Y_f/Y_S$ and $\eta = d_f/d_S$, where Y_S and Y_f are substrate and layer Young modulus respectively. The plus (or minus) sign depends on applied bending opposite to (or with) the built-in curvature.

Table 2 exposes the different values of strain applied on the 25µm thick Kapton & µ-Si TLM for each radii of curvature.

	Top surface strain calculation ($\varepsilon_{surface}$ %)
Radii curvature	**Kapton® (25 µm) + µC-Si (100 nm)**
R = 2.5cm	0.045
R = 2cm	0.056
R = 1.5cm	0.074
R = 1cm	0.112

Table 2. Top surface strain according to radii of curvature.

TLM structures as well as single strain gauges share the same technological process realized in clean room by photolithography (Figure 4). The TLM fabrication process starts by a cleaning step of a 10x10 cm² large and 25 µm thick PI substrate with acetone, alcohol and deionized water. The active layer, a 100 nm thick doped µ-Si film, is deposited by ICP-CVD and islands-like are patterned by Reactive Ion Etching (RIE) using a SF_6 plasma. A 300 nm thick aluminium layer (Al) is deposited by thermal evaporation and patterned by wet etching to form electrodes and test pads. The sample is subjected to a final thermal annealing at 180°C for 2h. This last step improves general µ-Si resistivity as well as ohmic contact between Al and µ-Si.

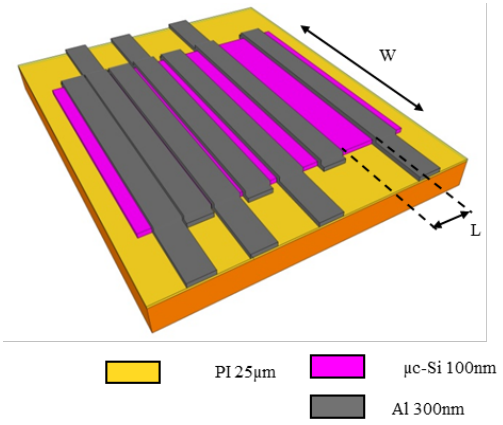

Figure 4. Schematic of a final TLM structure. Each structure is composed of 6 resistors, corresponding to 6 lengths *L* (5, 10, 20, 40, 80 and 160 µm). 4 different widths (*W*) are studied (1000, 500, 250 and 125 µm), which results in 24 different resistors.

This method using cylindrical bending test bench has been previously used to determine influence of mechanical stress in µ-Si Thin Film transistor TFTs [28] and has then been adapted to determine GF of µ-Si layers from PECVD for strain gauges development. PECVD µ-Si layers were then investigated, showing GF= -28 in the tensile domain and -37 in the compressive one [14] for a 50µm thick kapton substrate encapsulated in a 100nm thick nitride. In order to validate our test bench but with a 25µm thick substrate without nitride layers, TLM were performed using the already known PECVD µ-Si As doped layers [13]. These TLM presented a GF= -28 in tensile domain, and as expected PI thickness and nitride lack did not affect final GF final result.

The following GF measurements were performed with TLM using ICP-CVD µ-Si as active layer. The resistivity of µ-Si layer on PI substrate was calculated at 0.1 Ohm.cm, which is similar to PECVD resistivity level. Although resistivity level is not a key issue in static strain gauges, in case of applied dynamic pressure, a too high resistivity level will certainly induce a frequency limitation. After several TLM measurements under various applied stresses figure 5 shows the GF determination (slope) for µ-Si layer deposited by ICP-CVD at 600W with PH_3 doping at 185°C.

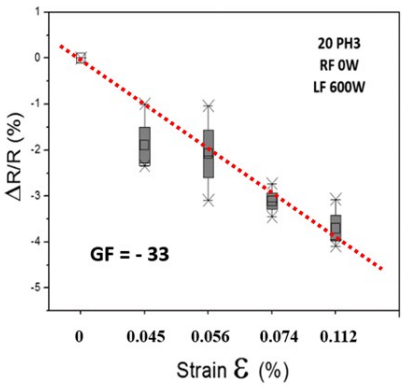

Figure 5. ICP-CVD µ-Si Gauge Factor determination by TLM structure deformation on bending test bench (Fig. 2) realised with 100nm µ-Si layers on 25µm Kapton.

These TLMs on 25 µm PI substrate exhibit a GF = -33 in the tensile range as shown in figure 5. This GF is slightly higher than PECVD one previously measured (-28), which validates the potentiality of ICP-CVD in thin film strain gauge sensors. This µ-Si GF value is similar with nc-Si:H issued from PECVD or Hot Wire Chemical Vapour Deposition HW-CVD process [29-30].

3. Dynamic measurement and investigation on strain gauges design.

The previous characterization systems used for GF determination or pressure mapping were not suitable for low pressure dynamic signal recording. Firstly, because it was based on probes with needles on the edge, it was not compatible with dynamic deformations, and secondly because of the range of applied pressure which was around 20 bar and do not fit with possible medical applications that need to detect signals at lower applied pressure.

So it was necessary to create a new test bench dedicated to dynamic deformations. Strain gauge designs were associated with deported connection path in order to drive away from several cm the connection area to active piezoresistive zone.

3.1 Dynamic test bench description:

It was decided to dynamically stress the strain gauges by using pneumatic signals. This solutions presents different advantages but the main one is to approach as close as possible the operating range of some targeted applications such blood pressure or heartbeat monitoring.

A pneumatic test bench has been developed based on a flow control system called Elveflow OB1 [31]. This equipment is based on piezoelectric regulators, enabling a flow control for

liquids or gases (Figure 6). Generally, Elveflow OB1 is used for microfluidic applications but in our case, it has been configured to be used with compressed air.

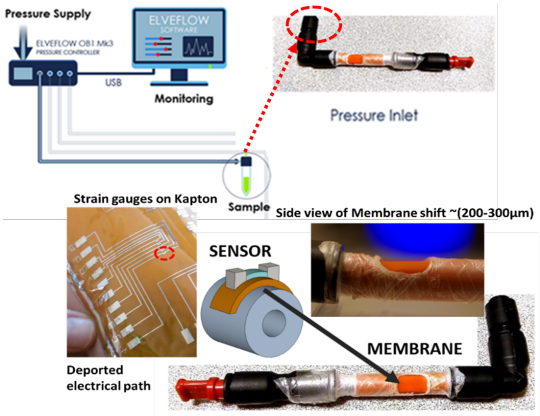

Figure 6. Schematic of the pneumatic test bench using Elveflow OB1 pressure machine [31], and rubber vibrating membrane where are set strain gauges.

In addition, it was necessary to create a platform to apply this pressure. For this goal, the sensor is placed onto a homemade vibrating rubber pipe whose shape changes when pulses are applied. As the sensor is completely attached to the membrane by a thin adhesive layer, the pressure pulse is transmitted to the sensor. The vibrating membrane is connected to the pressure supply machine whose outlet can be adjusted with a specific pressure range that can be modulated to create different shapes. The system is shown on Figure 6.

3.2 Acquisition system and signal processing:

The flexible sensor has been integrated with an Arduino Uno platform to manage the hardware/software interface (Figure 7). The chosen measurement system is based on a voltage divider circuit combining the flexible sensor with a variable reference resistance. The resulting signal is weak, and requires an amplification with a differential amplifier stage to reject DC signal coming from voltage divider. At the end, the output signal is filtered by a post FFT processing to reject the 50 Hz parasitic signal.

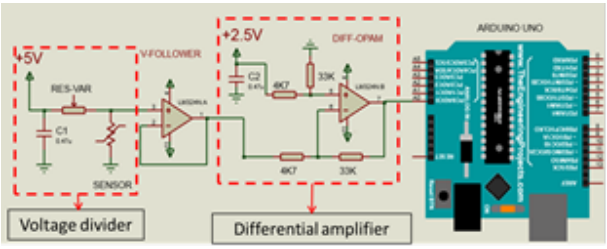

Figure 7. Acquisition system based on voltage divider with differential amplification before digital conversion realized by Arduino platform.

3.3 Investigation on Strain Gauges design:

First, dynamic responses of several designs have been investigated (Figure 8). Investigated strain gauges have been fabricated in a 2 deposition step process including a first µ-Si deposition by ICP-CVD, followed by patterning and etching by SF_6 RIE, after Al layer acting as connection path was deposited by Joule effect and patterned by wet etching.

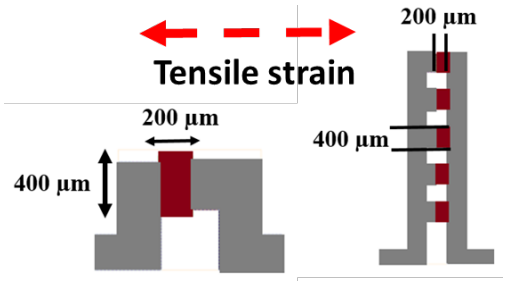

Figure 8. Design of the 2 strain gauges studied in dynamic, single strain gauge resistance (W/L 200/400µm) and the five parallel resistance strain gauge (µ-Si red, Al grey). Strain gauges were placed in a longitudinal way and stress by tensile strain.

Two main designs are exposed in figure 8. The single resistance (W/L=400/200µm) and five strain gauges in parallel. All these sensors are stuck on the pneumatic membrane of the pressure test bench by double sided adhesive. Electrical connections occur via deported paths to prevent any mechanical voids on metal connectors generated by the applied pressure.

These strain gauges have been stressed with various types of signals at different pressures. Sinusoidal, square and peak signals were send to analyse the different behaviour of gauges (figure 9).

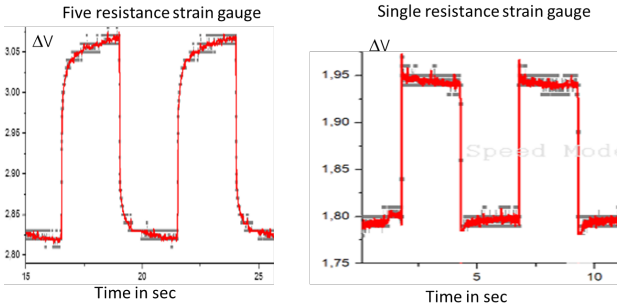

Figure 9. Behaviour of the 2 studied strain gauges stressed with 0.2Hz square signal of 200mbar amplitude pressure.

As it could be noticed figure 9, reactions of strain gauges submited to a square wave signal of 0.2Hz are quite different.

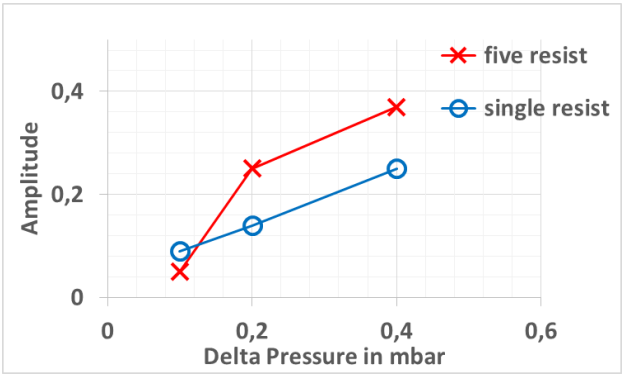

Figure 10. Amplitude variation of strain gauges response according to their design in case of square shape pressure signal applied.

Five resistance design provides a higher level of response at high pressure, but the single resistance provides a better one at low pressure as shown in figure 10. Single resistance responses are more linear over the studied pressure range. The leading time in

case of square wave signal applied is shorter with single resistance sensor (Figure 11). This implicates that single resistance design could cutof at a higher frequency pressure signal without degrading it.

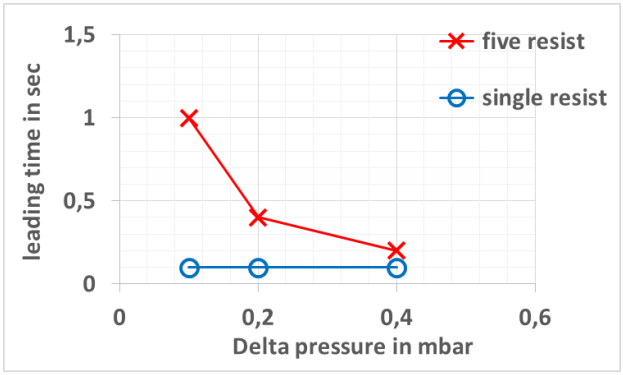

Figure 11. Evolution of leading time according to pressure and nature of strain gauge design, in case of square shape pressure signal applied.

It's interesting to notice the different behaviour of single resistance and five parallel resistances at low pressure. Both designs present advantages as well as weakness also. With a focus on selecting the best geometry, the two strain gauge designs have been studied according to the nature of signal but also submitted to reliability tests.

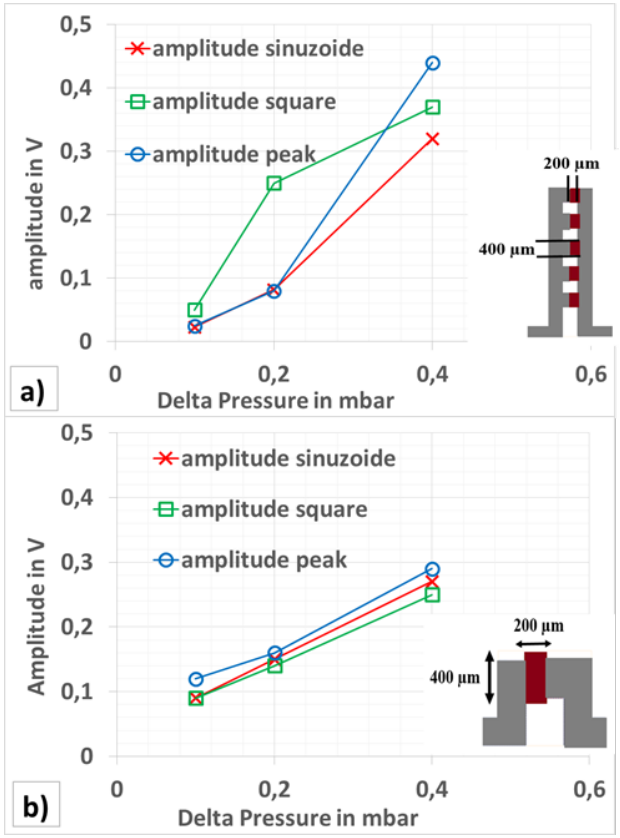

Figure 12. Comparison between five resistance a) and single strain gauge resistance b) performances according to the nature of applied pressure signal.

On these two designs, the five parallel resistances and the single resistance, some significant differences could be noticed on Figure 12.

For each type of signal applied, such as sinusoidal, square or peak, the single square strain gauge responds with a good linearity over the investigated pressure range investigated. Moreover, the value of response is similar for any type of signal. In case of the five resistance strain gauge, at high pressure, sensitivity is better but different depending on nature of signal, and at low pressure, the sensitivity is low. For sinusoidal and peak signals, single resistance transducing is most efficient below approximately 0.3 mbar. In the case of transducing a complex signal combining pulses, waves and square shapes, the single resistance strain gauges could certainly reach better accuracy and provide less distortions due to its better response uniformity of response over different signal shapes (Fig 12b).

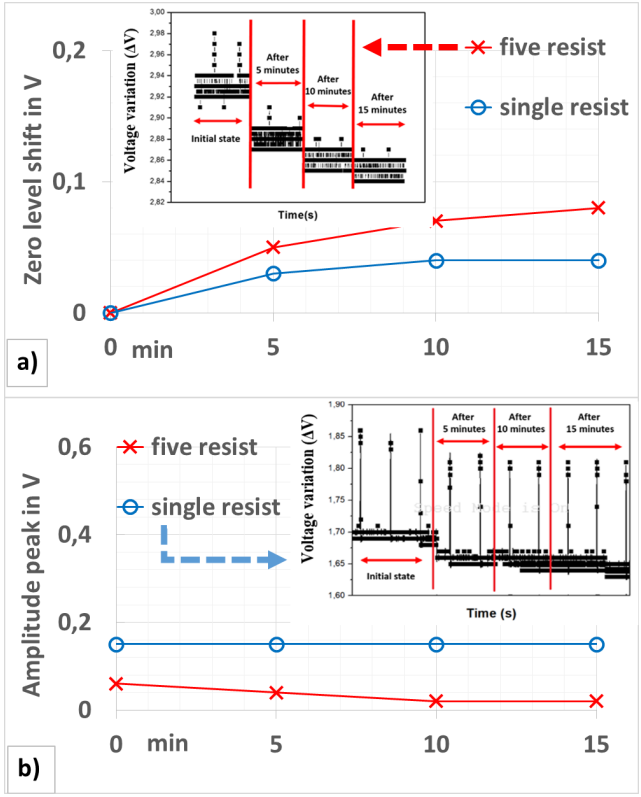

Figure 13. 15 minutes of reliability tests showing the zero level shift a) and amplitude variation b) according to the design of strain gauge.

To conclude on strain gauges shape investigation, some reliability tests have been performed. They consisted in applying a 200mbar pulsed peak (width peak 0.3s) at frequency of 0.2 Hz during fifteen minutes and controlling the drift of sensor signal. Again in this configuration, the single resistance design showed less drift as well in terms of zero level shift than peak amplitude drift (Figure 13). According previous TLM tests, it appeared that cracks could be generated on µ-Si layers deposited on 50µm thick PI substrate when it was bent on low radii curvature cylinder (<5mm). In present case with a 25µm PI substrate applied pressure is very weak and drift of signal should not be directly induce by mechanical voids but it could rather come from different origins like self-heating of the structure, or degradation of the adhesive layer between strain gauge and the rubber pipe.

After these tests, it could be conclude some important points. In all cases, the resistance (W/L 400/200µm) shows good transducing characteristics. According to the pressure range, it might be interesting to use single resistance geometry (at low pressure) and rather a combination of several parallel resistances at higher pressure. In addition both design could be combined to extend the sensitivity on pressure range. In any case, the single resistance geometry responds better in terms of frequency and reliability, and also provides a better spatial resolution. This last argument is essential for the array sensors realization.

4. Strain Gauges array fabrication and mechanical tests.

In a next step, single resistance strain gauges have been integrated into a 5 by 5 line column array.

4.1 Strain Gauges array design and fabrication:

This array have been performed on a 25µm thick kapton substrate, it consisted on a first 100nm µ-Si layer deposited by ICP-CVD and patterned by SF_6 Reactive Ion Etching (RIE). A first 200nm layer of Al metal 1 is then deposited and patterned, followed by a 200nm inter-metal ICP-CVD SiO_2 layer etched by CF_4 RIE. The array is completed by a last 200nm Al metal deposition to perform metal 2 layer. The final array presents a 5mmx5mm active area (Figure14). This structure could achieve two principal goals. Firstly, by providing several identical sensors, it brings redundancy and improves the final reliability of the sensor allowing a better statistical processing. Secondly, in case of applied pressure with a gradient or issue from a localized concentrated point, it could be interesting to provide a pressure mapping with good spatial accuracy (<1mm).

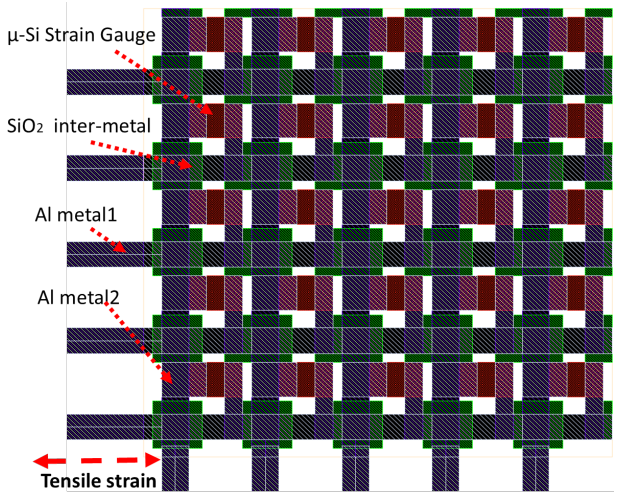

Figure 14. Design of ICP-CVD processed 25 strain gauges array, µ-Si active layer (red), SiO_2 inter-metal (green) and Al1 & Al2 connection path (blue).

This matrix has been implemented on our test bench and submitted to different types of signals, as peak signal or more complex one. In the following experiments, no multiplexing system (MUX) has been used so it means that every sensor have been measured separately, one by one.

4.2 Strain Gauges array tested by pulse peak:

In a first test, matrix has been stressed with 200mbar pulses at 0.2Hz. Results are exposed in Figure 15.

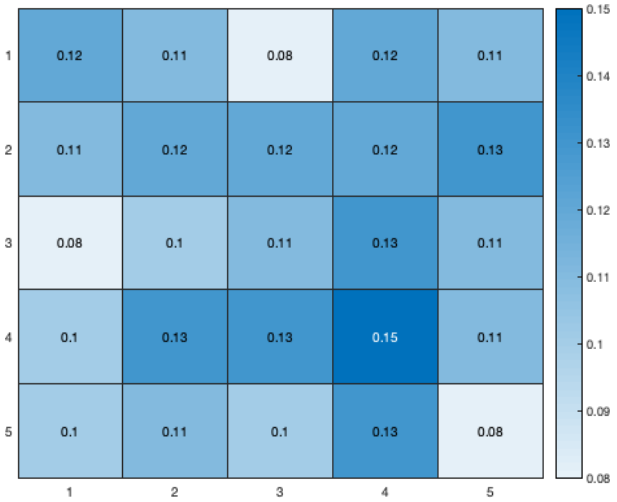

Figure 15. Amplitude measured in V by the strain gauge array with 200mbar peak pulse applied. The C4-L4 sensor reaches maximum sensitivity, as shown previously in Figure 12.

Average amplitude of response within the matrix is 112mV with a standard deviation of 17mV. This result can be compared with the sensitivity obtained under the same condition with single resistance sensor (150mV in Fig 12). In this case, the matrix design has no significant effect on the overall sensitivity of the system. It is in fact, a quite good result because the array design usually impacts individual sensor response by adding parasitic resistance and capacitance. One sensor (C4-L4) even achieves the same sensitivity as in single resistance strain gauge tests.

4.3 Behaviour and reliability with complex signal applied:

During a second test, without removing our array from the test bench, the strain gauge array has been stressed with a more complex signal. The Elveflow system is able to generate complex signals issue from a coded script. In our case, we re-used a script from an ECG shape just to demonstrate the ability of our sensor array to transduce without to many distortion a quite complex signal. The complex signal generated presents a maximum pressure peak of 400mbar associating two other smaller sinusoidal parts. The signal was repeated at 0.2Hz frequency as described in Figure 16.

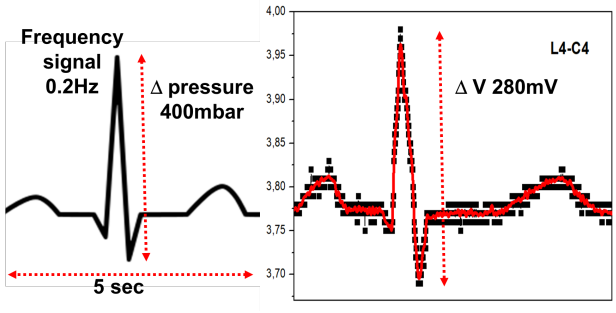

Figure 16. Structure of the complex signal generated by the Elveflow generator pressure and applied to the array.

This low frequency was decided in the first instance because the Elveflow pressure air generator could not generate complex signal at high frequency without losses in signal accuracy. It can be noticed from figure 17 that signal issue from best sensor of the array (i.e C4-L4) still responds linearly with a amplitude peak of

280mV as expected in the previous tests (figure 12). Figure 17 shows the response of the 25 sensors of our array after quick post treatment filtering. Sensors of the array that correctly reproduce the three parts of the signal without showing drift of the base level or too much noise have been surrounded to highlight the good level of reliability within matrix. Indeed, 20 sensors (80%) reproduced the entire signal without distortion. All failed sensors come from the edges of the array and are quite far from the best C4-L4 one. This distance and perhaps some voids in the adhesive process between PI flexible substrate and pneumatic membrane could also explain the bad transduction quality in these five cases. Finally, the array was stressed during 90min with loading/off-loading test using a 0.2 Hz 200mbar amplitude peak signal (peak width 0.3s). Percentages of resting resistance shift after the fatigue test are visible in figure 17. It is interesting to notice in central array a very small drift instead of a very significant shift on the edges, especially on the two sides where electrical connections occur. This seems to link the reliability to the current density through µ-Si layers or perhaps to effects of electro migration on Al paths.

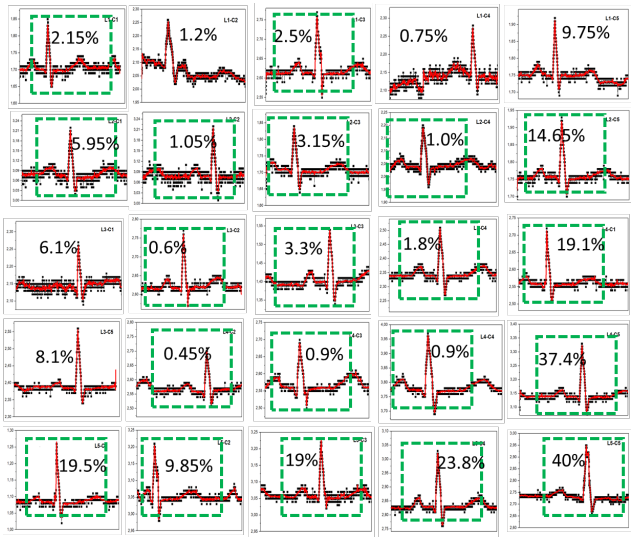

Figure 17. Recording of complex signal transducing by the 25 sensor array. Distortion-free signals are highlighted in green. After 90 min of loading/off-loading tests, resistance variations are expressed as a percentage.

The µ-Si strain gauge array has been tested using different kind of signals at various pressures. It results that array design provides 25 similar strain gauges which all react in a similar way to pulse peak pressure; in fact just 15% of standard deviation have been measured for a 200mbar peak pulse applied pressure. In case of complex signal transducing, 80% of sensors reproduce exactly the signal without distortion. The array provides redundancy as well as possibility to select best sensor to improve detection. All these tests demonstrate the major interest of array design combined with µ-Si strain gauges on flexible substrates, especially in pressure monitoring applications.

5. Test set up improvement application to blood pressure monitoring.

Previous experiments aimed at characterizing the sensor behaviour under dynamic stress. They revealed some promising effects in terms of sensitivity and signal transduction. In order to study in more details the operational interest of the µ-Si/flexible technology, another test set up has been implement to closely simulate a blood pressure monitoring application. On this test bench, we plug a single resistance strain gauge to investigate its performance in a more realistic environment.

5.1 Pneumatic test bench dedicate to blood pressure:

Based on the principle of previous test bench, an artificial wrist was made of silicone with two bones made of glass to simulate radius bone and ulnar bone. A channel has been performed inside silicone to simulate artery and linked to the Elveflow pressure generator (Figure 18). With this set up, it can be possible to simulate the flesh mechanical properties as well as the impact of bones on blood pressure waves inside the arm. This artificial wrist have been realised by Cherry Biotech for their own research activities and adapted to our specific purpose.

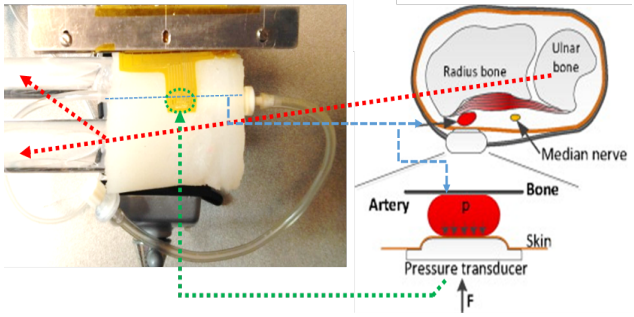

Figure 18. Artificial silicone wrist with 2 parts of bones-simulating glass and a micro fluidic channel as artery (blue). Strain gauges are sticked at the vicinity of artery to record the simulated blood pressure.

5.2 Electrical set up and signal processing improvement:

First set up was based on voltage divider combined with an amplification stage, using analogic converter of the Arduino platform. The voltage divider circuit has been replaced by a Wheatstone bridge circuit to reject DC signal. Analog Digital Converter of Arduino is a 10-bits ADC leading to a low resolution measurement. This ADC has been replaced with an Analogic Digital Converter ADS126 with a 32bit resolution and integrating a low noise filter. This configuration reduces the general noise on the measurement system and as a result provides a better accuracy to detect low pressure variation such as those observed in case of blood pressure measurement.

5.3 Low blood pressure signal simulation and acquisition:

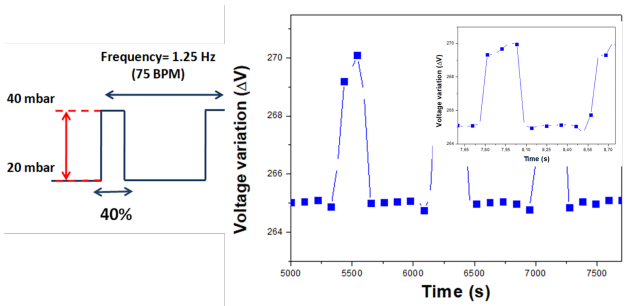

Figure 19. 75 BPM signal recorded by single strain gauge with improved low noise electrical set up. Applied signal simulates a weak 20mbar blood overpressure drive in the artificial wrist.

In this last part, we generate in our artificial wrist a 20mbar delta pressure signal at 1.75Hz (75 BPM Beats Per Minute) simulating a systolic/diastolic pressure gap of 15mm Hg (low range). Results are provided in Figures 19 and 20.

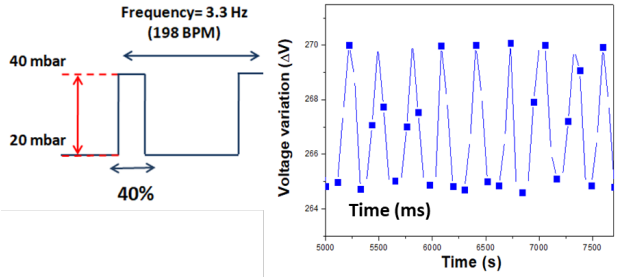

Figure 20. 198 BPM signal recorded by single strain gauge with improved low noise electrical set up. 20mbar overpressure signal is still noticeable although sample rate is too low to assure a good accuracy in signal transduction.

In both cases, the 20mbar of pulse pressure have been detected resulting from 5mV of voltage shift (figure 19) which is consistent with previous tests (figures 12-15-17). The system was able to track variation until high frequency of simulated blood pressure signal (198 BPM in figure 20) even if in this last case, accuracy of signal was degraded by the sampling capacity of Arduino rather by the sensor itself.

6. Conclusions

This article presents µ-Si Strain gauges perform on 25µm thick PI (Kapton) flexible substrate. The active layer of the µ-Si sensors were issued from a low temperature ICP-CVD process. Using the background available from PECVD low temperature µ-Si, gauge factor was studied for this material using cylindrical strain test bench. GF has been measured at -33 in tensile domain, which is slightly higher than one calculated previously in PECVD for µ-Si as well.

After this static characterization, a dynamic test bench was set up to analyse the behaviour of µ-Si strain gauges. This test bench was based on a compressed air signal generator. This system, originally designed for micro-fluidic application, is suitable enough to generate small pressure signals. These pressure pulses or waves were sent inside a pneumatic pipes with a rubber part allowing deformation at the sensor location.

Different designs of gauges have been investigated in terms of amplitude but also leading time or response linearity. Results show clearly that in case of dynamic low pressure signal, small µ-Si resistances (W/L 400/200µm) offer best characteristics.

Using the most efficient design, an array of 25 sensors have been performed using two metal layers and ICP-CVD inter-metal silicon oxide. This array was tested on the pneumatic test bench and all sensors responded to the applied pulses with a good sensitivity dispersion (<20%), the best part of the array reaching same sensitivity that single one previously. The array was also tested with complex signals that were also well transduced. At the end, some reliability tests showed low resistance shifts at the centre of the array, but high resistance drift at the edge and especially where electrical connections occur. This array design could be used for different purposes, either to increase reliability by averaging signals, or as discriminant non-valid sensor either by creating a pressure sensor map with a sub-millimetre accuracy.

Finally, another pneumatic test bench was implemented using an artificial silicone wrist including a channel at the vicinity of the silicone surface with two bones to simulate the behaviour of pressure waves in arteries. The electrical set up was improved by using low noise ADC and, by this way, 20mbar pressure signal at 75 BPM and 198 BPM were measured with quite good accuracy. This demonstrating the main interest of this technology in medical application.

In association with a high quality sampling system and MUX system, a µ-Si sensor array performed on a flexible 25µm PI Kapton substrate could be a major device for blood pressure monitoring. In fact, with its low invasive effect and its integrated possibilities, it could be an interesting alternative to existing system.

7. Acknowledgments

All tests and devices have been performed on the NanoRennes platform with the support of the CNRS French national research agency and the project CPER Sophie/STIC&Onde. Artificial Wrist was realized at Cherry Biotech Rennes.

8. References

[1] T. Someya, Y. Kato, T. Sekitani, S. Iba, Y. Noguchi, Y. Murase, H. Kawaguchi, T. Sakurai, “Conformable, flexible, large-area networks of pressure and thermal sensors with organic transistor active matrixes”, Proc. Nat. Acad. Sci. 102 (35) (2005) 12321-12325

[2] S. Jung, T. Ji, V.K. Varadan, “Point of care temperature and respiration monitoring sensors for smart fabric applications”, Smart Mater. Struct. 15 (2006) 1872-1876

[3] D.H. Kim, N. Lu, R. Ma, Y.S. Kim, R.H.Kim, S. Wang, J. Wu, S.M.Won, H. Tao, A.Islam, K.J. Yu, T. Kim, R. Chowdhury, M. Ying, L. Xu, M. Li, H.J. Chung, H. Keum, M. McCormick, P. Liu, Y.W. Zhang, F.G. Omenetto, Y. Huang, T. Coleman, J.A. Rogers, “Epidermal electronics”, Science 333 (6044) (2011) 838-843

[4] R.B. Katragadda, Y. Xu, “A novel intelligent textile technology based on silicon flexible skins”, Sens. Actuators A 143 (2007) 169-174

[5] E. Fallettaa, P. Costab, C. Della Pinaa, S. Lanceros-Mendez, “Development of high sensitive polyaniline based piezoresistive films by conventional and green chemistry approaches”, Sens. Actuators A 220 (2014) 13–21

[6] A. Bessonova, M. Kirikovaa, S. Haqueb, I. Gartseeva, M.J.A. Bailey, “Highly reproducible printable graphite strain gauges for flexible devices”, Sens. Actuators A 206 (2014) 75–80

[7] D. Lee, H.P. Hong, M.J. Lee, C.W. Park, N.K. Min, “A prototype high sensitivity load cell using single walled carbon nanotube strain gauges”, Sens. Actuators A 180 (2012) 120–126

[8] N. Lu, C. Lu, S. Yang, J. Rogers, “Highly Sensitive Skin-Mountable Strain Gauges Based Entirely on Elastomers”, Adv. Funct. Mater. 22 (19) (2012) 4044-4050

[9] S. Yang, N. Lu, “Gauge factor and stretchability of silicon-on-polymer strain gauges”, Sensors 13 (7) (2013) 8577-8594

[10] P.J. French, A.G.R. Evans, “Piezoresistance in polysilicon and its applications to strain gauges”, Solid State Electron. 32 (1) (1989) 1-10

[11] H. Gleskova, S. Wagner, W. Soboyejo, Z. Suo, “Electrical response of amorphous silicon thin-film transistors under mechanical strain”, J. Appl. Phys. 92 (2002) 6224-6229

[12] P. Roca i Cabarrocas, “Plasma enhanced chemical vapor deposition of amorphous, polymorphous and microcrystalline silicon films”, J. Non-Cryst. Solids. 266–269(2000) 31–37

[13] K. Kandoussi, C. Simon, N. Coulon, K. Belarbi, and T. Mohammed-Brahim, “Nanocrystalline silicon TFT process using silane diluted in argon–hydrogen mixtures”, J. Non-Cryst. Solids 354 (19) (2008) 2513–2518

[14] Y. Kervran, O. De Sagazan, S. Crand, N. Coulon, T. Mohammed-Brahim, O. Brel, “Microcrystalline silicon: strain gauge and sensor arrays on flexible substrate for the measurement of high deformations”, Sens. Actuators A: Phys. 236 (2015) 273-280

[15] H. P. Zhou , D.Y. Wei, S. Xu, S.Q. Xiao, L.X. Xu, S.Y. Huang, Y. N. Guo, S. Khan, M. Xu, “Crystalline silicon surface passivation by intrinsic silicon thin films deposited by low-frequency inductively coupled plasma”, J. Appl. Phys. 112 (1) (2012) 013708-9

[16] M. Goto, H. Toyoda, M. Kitagawa, T. Hirao, H. Sugai, “Low Temperature Growth of Amorphous and Polycrystalline Silicon Films from a Modified Inductively Coupled Plasma”, Jpn. J. Appl. Phys. 36 (6A) (1997) 3714-3720

[17] C.-H. Shen, J.M. Shieh, J.Y. Huang, H.-C. Kuo, C.-W. Hsu, B.-T. Dai, C.-T. Lee, C.L. Pan, F.L. Yang, “Inductively coupled plasma grown semiconductor films for low cost solar cells with improved light-soaking stability”, Appl. Phys. Lett. 99 (3) (2011) 033510-3

[18] S. Q. Xiao, S. Xu, H.P. Zhou, D.Y. Wei, S.Y. Huang, L.X. Xu, C.C. Sern, Y.N. Guo, S. Khan , “Amorphous/crystalline silicon heterojunction solar cells via remote inductively coupled plasma processing”, Appl. Phys. Lett. 100 (23) (2012) 233902 (3pp)

[19] Q. Cheng, S. Xu, J. Long, S. Huang, and J. Guo, “Homogeneous nanocrystalline cubic silicon carbide films prepared by inductively coupled plasma chemical vapor deposition”, Nanotechnology 18 (46) (2007) 465601 (6pp)

[20] T. Frischmuth, M. Schneider, D. Maurer, T. Grille, and U. Schmid, “Inductively-coupled plasma-enhanced chemical vapour deposition of hydrogenated amorphous silicon carbide thin films for MEMS”, Sens. Actuators Phys. 247 (2016) 647–655

[21] C. Jeong, Y.B. Kim, S.-H Lee, J.H. Kim, “Preparation of Born-Doped a-SiC:H Thin Films by ICP-CVD Method and to the Application of Large-Area Heterojunction Solar Cells”, Journal of Nanoscience and Nanotechnology 10 (5) (2010) 3321-3325

[22] C.H. Jeong, M.S. Jeon, K. Koichi, “Electrical Properties of Boron and Phosphorus Doped μc-Si: H Films using Inductively Coupled Plasma Chemical Vapor Deposition Method for Solar Cell Applications”, Transactions on Electrical and Electronic Materials 9 (1) (2008) 28-32

[23] G. Nogay, E. Özkol, S. Ilday, and R. Turan, “Structural peculiarities and aging effect in hydrogenated a-Si prepared by inductively coupled plasma assisted chemical vapor deposition technique”, Vacuum 110 (2014) 114–120, Dec. 2014.

[24] S. Grover, “Effect of Transmission Line Measurement (TLM) Geometry on Specific Contact Resistivity Determination”, thesis Rochester Institute of Technology, 2016

[25] H. Gleskova, S. Wagner, Z. Suo, “Failure resistance of amorphous silicon transistors under extreme in-plane strain”, Appl. Phys. Lett. 75 (1999) 3011-3013

[26] Technical Data sheet, DuPont Kapton HN (available online)

[27] J. Gaspar, A. Gualdino, B. Lemke, O. Paul, V. Chu, J.P. Conde, “Mechanical and piezoresistive properties of thin silicon films deposited by plasma-enhanced chemical vapor deposition and hot-wire chemical vapor deposition at low substrate temperatures”, J. Appl. Phys. 112 (2) (2012) 024906-14

[28] H. Dong, Y. Kervran, N. Coulon, O. de Sagazan, E. Jacques, T. Mohammed-Brahim , “Highly flexible microcrystalline silicon n-type TFT on PEN bent to a curvature radius of 0.75 mm ”, IEEE Transactions on Electron Devices 62 (10) (2015) 3278-3284

[29] P. Alpuim, J. Gaspar, P. Gieschke, C. Ehling, J. Kistner, N.J. Goncalves, M.I. Vasilevskiy, O. Paul, “Study of the piezoresistivity of doped nanocrystalline silicon thin films”, J. Appl. Phys. 109 123717 (2011)

[30] P. Alpuim, S.A. Filonovich, C.M. Costa, P.F. Rocha, M.I. Vasilevskiy, S. Lanceros-Mendez, C. Fria, A. Torres Marques, S. Roares, C. Costa, “Fabrication of a strain sensor for bone implant failure detection based on piezoresistive doped nanocrystalline silicon”, J. Non-Cryst. Sol. 354 (2008) 2585–2589

[31] Datasheet ‘OB1 - 4 channels microfluidic flow controller’, *Elveflow*.